

pubs.acs.org/JACS Article

Electrochemical Deposition of an *N*-Heterocyclic Carbene (NHC) Functionalized CO₂ Reduction Catalyst on Au Electrodes

Lydia R. Weddle, Jan Paul Menzel, Pablo E. Videla, Emile E. DeLuca, Hao Fan Su, Hao Chen, Joseph M. Palasz, James M. Taylor, Zhuoran Long, Victor S. Batista,* and Clifford P. Kubiak*



Cite This: https://doi.org/10.1021/jacs.5c11267



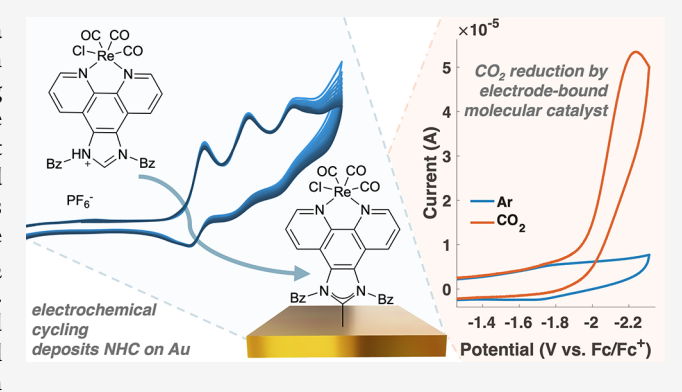
ACCESS I

III Metrics & More

Article Recommendations

s Supporting Information

ABSTRACT: Electrode-bound molecular species provide a powerful platform for probing interfacial electric field effects on immobilized catalysts. However, common surface anchoring groups such as thiols and isocyanides largely undergo reductive stripping before catalytic onset. Herein, we demonstrate that stronger N-heterocyclic carbene (NHC) anchoring groups extend the accessible electrochemical window for studying catalysts immobilized on electrode surfaces. Specifically, we report the covalent attachment of an NHC-functionalized rhenium CO₂ reduction catalyst on gold via electrochemical deposition. Voltammetric characterization, polarization modulation infrared reflection absorption spectroscopy (PM-IRRAS), computational modeling, and X-ray photoelectron spectroscopy (XPS) confirm



the formation of an electrochemically assembled monolayer that demonstrates persistence through large cathodic excursions and electrocatalytic CO_2 reduction.

■ INTRODUCTION

Molecular catalysts for CO_2 reduction (e.g., $Re(bpy)(CO)_3Cl$) have well-defined active sites which are studied closely by established spectroscopic and electrochemical techniques. 1-8 Their electronic properties can be precisely tuned through the inductive effects of ligand substitution, enabling high selectivity for desired products such as CO. 1,9 By contrast, heterogeneous catalysts for CO₂ reduction (e.g. Cu) can drive CO₂ reduction to $n > 2e^-$ products such as ethylene, but the diversity of surface sites and their variation over time can thwart mechanistic investigations. ^{10–12} In recent years, an increasing body of research has emerged focusing on molecular electrocatalysts immobilized on electrode surfaces, including silicon 13,14 and graphitic supports. 15-19 Surendranath and coworkers published a series of these studies where molecular catalysts are covalently conjugated onto carbon electrodes through pyrazine bridges. $^{20-25}M(bpy-R)(CO)_3X$ (M = Re, Mn X = Cl, Br) complexes have also been adsorbed through π interactions onto multiwalled carbon nanotubes (MWCNTs), where exceptional rate and selectivity for CO₂ reduction products was recorded even in aqueous electrolyte where hydrogen evolution should compete.26-28 The marked modulation—often improvement—in the performance of many molecular catalysts on carbon nanotubes as compared to their homogeneous counterparts suggest that electrode proximity, electron transfer dynamics, and interfacial electric fields play significant roles and warrant deeper investigation.

Yet, spectroscopic observation of these effects is compromised by the absorbing and structurally complex nature of carbonaceous supports. To address these challenges, molecular catalysts immobilized on spectroscopically accessible planar substrates provide a valuable window to observe the behavior of surface-bound catalysts as distinct from their homogeneous counterparts.

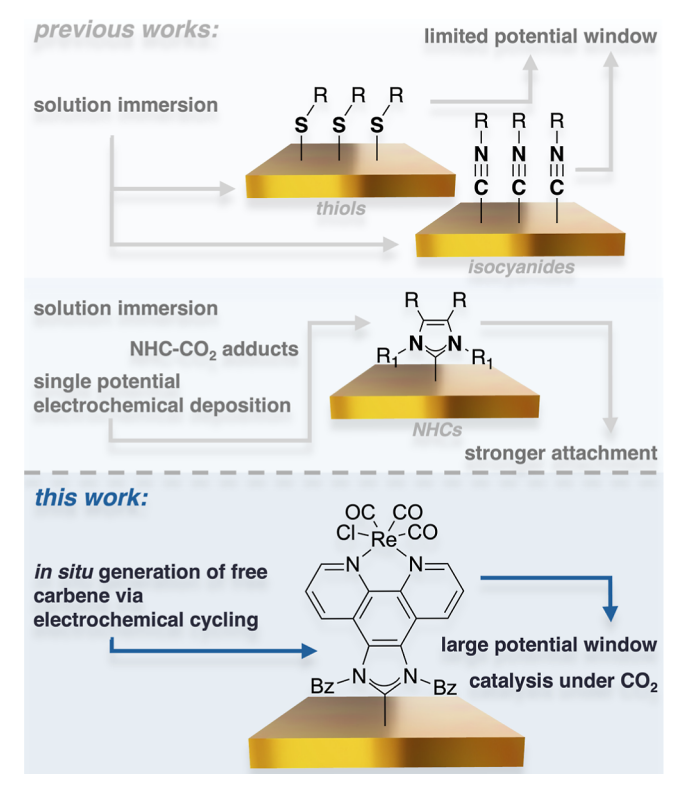
Understanding the microenvironment at electrode/electrolyte interfaces remains a key challenge in interfacial catalysis. A common approach involves monitoring self-assembled monolayers (SAMs) containing vibrational probes on reflective electrode surfaces by *in situ* spectroelectrochemistry, often with the support of computational modeling. Seminal work in this area by Dawlaty and co-workers used substituted and surface-bound 4-mercaptobenzonitrile to track vibrational frequency shifts of signature $\nu(\text{CN})$ stretches, and quantitatively linked ligand electronic effects and applied potential to field-induced changes in electrode-bound molecules. Shortly thereafter, Baik and co-workers introduced the concept of the "electro-inductive" effect, demonstrating that applied bias

Received: July 3, 2025 Revised: October 20, 2025 Accepted: October 21, 2025



could influence chemical and catalytic transformations of surface-bound *substrates*.³⁴ Despite these advances, realizing a catalytically relevant, covalently tethered monolayer of molecular catalysts on a spectroscopically accessible Au electrode surface that remains stable over a wide enough potential window to study operando has only been possible under exotic conditions.³⁵ This limitation stems from the stability of common gold linkages (i.e., thiols, isocyanides) over large cathodic excursions (Scheme 1). For example,

Scheme 1. Molecular Immobilization Motifs on Au Electrodes^a



^aUbiquitous thiol- and isocyanide-based self-assembled monolayers are typically formed through immersion of the electrode in a solution of the desired molecule with corresponding functional group. NHCbased attachment strategies include immersion in solutions containing HCO₃⁻ salts or other base, NHC-CO₂ adducts, and electrochemical deposition at a fixed potential. The present work reports an electrochemical deposition technique for an NHC-functionalized molecular CO₂ reduction catalyst wherein cathodic cycling generates a satisfactory monolayer that endures large potential excursions and exhibits catalytic current enhancement under CO₂.

immobilization of the Re(bpy)(CO)₃Cl catalyst on Au electrodes via thiol linkage yielded a monolayer exhibiting pronounced field-induced modulation of the electronics of the metal center: Stark shifts of v(CO) bands were ~4 times greater than achievable by installation of electron-donating and -withdrawing substituents at the 4,4′ position of the bipyridine. Significantly, the thiol-bound monolayer stripped from the electrode at potentials well positive of the first reduction of the catalyst. A key goal here is to develop electrode-anchored molecular catalysts that remain attached under turnover conditions to spectroscopically observe the catalysts operando.

Crudden and co-workers recently introduced an "ultrastable" method for gold surface functionalization using N- heterocyclic carbenes (NHCs), demonstrating superior durability compared to traditional thiol and isocyanide anchoring moieties.³⁶ Building on this, we report the covalent attachment of an analogue of Re(bpy)(CO)₃Cl to a gold electrode via an NHC linker. Grafting is achieved by an electrochemical cycling method that reductively couples the NHC moiety to gold. The monolayer is characterized via cyclic voltammetry, polarization modulation infrared reflection absorption spectroscopy (PM-IRRAS), X-ray photoelectron spectroscopy (XPS), and by ICP-MS elemental analysis. Catalytic current is observed under CO₂ at potentials positive than that observed for blank Au and at an apparent rate faster than the catalyst in solution. Signal from the catalyst persists over large cathodic excursions and controlled electrolysis experiments under catalytic conditions, making this system a promising platform for spectroscopic observation of the Re CO₂ reduction catalyst at electrocatalytically relevant poten-

RESULTS & DISCUSSION

Characterization of Molecular CO2 Reduction Catalyst. Motivated by the dramatic field-induced shifts observed in the $\nu(CO)$ stretches of thiol-bound Re(bpy)(CO)₃Cl on Au,³¹ we designed a ligand framework enabling a more robust surface attachment: 1,3-dibenzyl-1H-imidazo[4,5-f][1,10]phenanthrolin-3-ium (hereafter referred to as phen-NHC), which bears distal NHC and polypyridyl moieties. Imidazophenanthroline scaffolds have seen prior use in photochemical sensing (including with Re, Ru)³⁷ and Re(I)-phenanthroline complexes are effective CO₂ reduction catalysts which provide a suitable molecular comparison for the heterogenized species.³⁸ Phen-NHC was prepared and metalated to yield the target [Re(phen-NHC)(CO)₃Cl][PF₆] (Figure 1) species as described and characterized in the Supporting Information. Cyclic voltammetry (CV) of [Re(phen-NHC)(CO)₃Cl][PF₆] (hereafter referred to as [Re(phen-NHC)(CO)₃Cl]⁺) was performed under Ar and CO₂ as a baseline for the behavior of the corresponding surface-attached species (Figure S4).

Five distinct reduction features are observed in the homogeneous cyclic voltammetry of Re(phen-NHC)-(CO)₃Cl]⁺ under an inert atmosphere (Figure 1, Table S2). In analogous Re bipyridine and phenanthroline systems, the first and second reductions are typically assigned as ligand and rhenium centered, respectively. 1,3,38 In bipyridyl complexes bearing electronically neutral and electron-donating substituents, the second reduction generates the catalytically active $[Re(bpy)(CO)_3]^-$ species, where the two electrons required for the transformation of CO₂ to CO are distributed between an admixture of the Re d_{z2} and ligand π^* orbital.^{5,39} In the present complex, each redox feature exhibits varying degrees of quasireversibility, indicative of delocalized metal-ligand orbital character and competing solution-phase equilibria. The first reduction feature of [Re(phen-NHC)(CO)₃Cl]⁺ is only partially reversible (Figure S3), and while scanning beyond the second reduction reveals a small oxidative wave on the reverse sweep (ca. -300 mV vs Fc/Fc⁺) characteristic of the oxidation of a Re⁰-Re⁰ dimer known to form in solution after the reduction of the Re^I state to Re^{0,4,7,40,41} catalytic current enhancement under CO2 coincides with the third reduction the complex, rather than the second, as observed previously in bipyridyl-ligated complexes with strongly electron-withdrawing substituents. This deviation points to unique electronic structure contributions from the phen-NHC scaffold. We

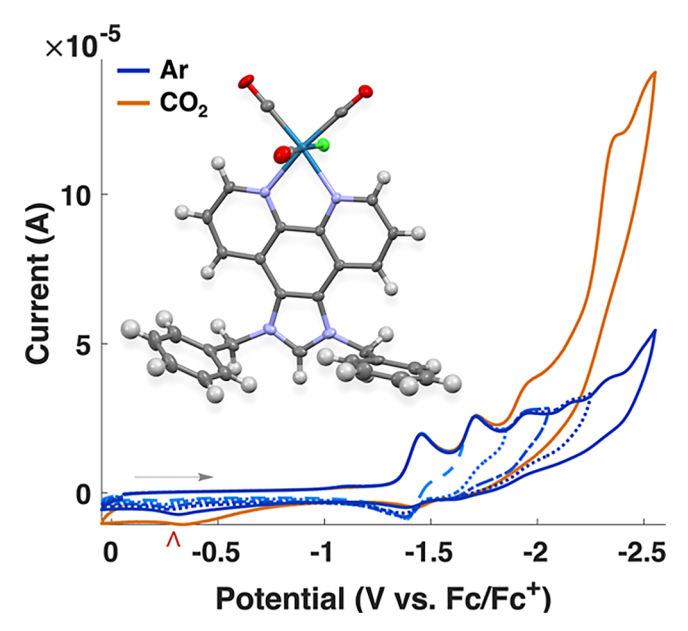


Figure 1. Crystal structure and CV of [Re(phen-NHC)(CO)₃Cl]-[PF₆]. Crystals were grown by vapor diffusion of diethyl ether into a concentrated acetonitrile solution of the complex. PF₆⁻ counterion omitted for clarity. Homogeneous electrochemistry under Ar (blue) and CO₂ (orange) of [Re(phen-NHC)(CO)₃Cl]⁺ in 100 mM TBAPF₆/ACN at a scan rate of 100 mV/s. The first two reductions are assigned as initially ligand-centered. The third reduction corresponds to the transformation to the catalytically active species under CO₂. The reverse oxidative wave (\wedge) is characteristic of Re⁰-Re⁰ dimer oxidative cleavage.

performed DFT calculations to assign these redox events and provide a more granular understanding of the electronics of [Re(phen-NHC)(CO)₃Cl]⁺ (see Supporting Information). These computations support: (1) that the first reduction of [Re(phen-NHC)(CO)₃Cl]⁺ is ligand-centered; (2) Cl⁻ ligand dissociation occurs upon the second reduction of [Re(phen-NHC)(CO)₃Cl]⁺; (3) that the third reduction is highly delocalized over the Re center and the phenanthroline backbone; (4) a formal rhenium-centered reduction does not occur until the fourth reduction (Figure S28). Therefore, we propose that the electron introduced at the third reduction feature of [Re(phen-NHC)(CO)₃Cl]⁺ travels via an interaction between the π -system of the ligand and through the metal center to initiate CO₂ binding and activation.

A more intricate reduction pathway is captured on the timescale of spectroelectrochemical (SEC) measurements under an inert atmosphere (Figure 2, detailed methods are provided in the Supporting Information). As electron density is added to the [Re(phen-NHC)(CO)₃Cl]⁺, the stretches of the facial tricarbonyl modes of the complex exhibit a red shift due to an increase in the strength of backbonding interactions.⁴ A formal reduction of the rhenium center is expected to shift the symmetric $\nu(CO)$ stretch by ~40 cm⁻¹,⁴² significantly larger than that for a ligand-based reduction (i.e., localized on phenanthroline or aryl imidazolium moiety). In agreement with DFT and voltammetric analysis, IR SEC of [Re(phen-NHC)(CO)₃Cl]⁺ under inert conditions supports three apparent ligand-dominated reductions, along with the formation of the Re⁰-Re⁰ dimer observed in CV as a minor species. The first spectral shift is very modest - only 2 cm⁻¹; the process responsible is discussed in detail in the section below. The second reduction of the complex produces a 21

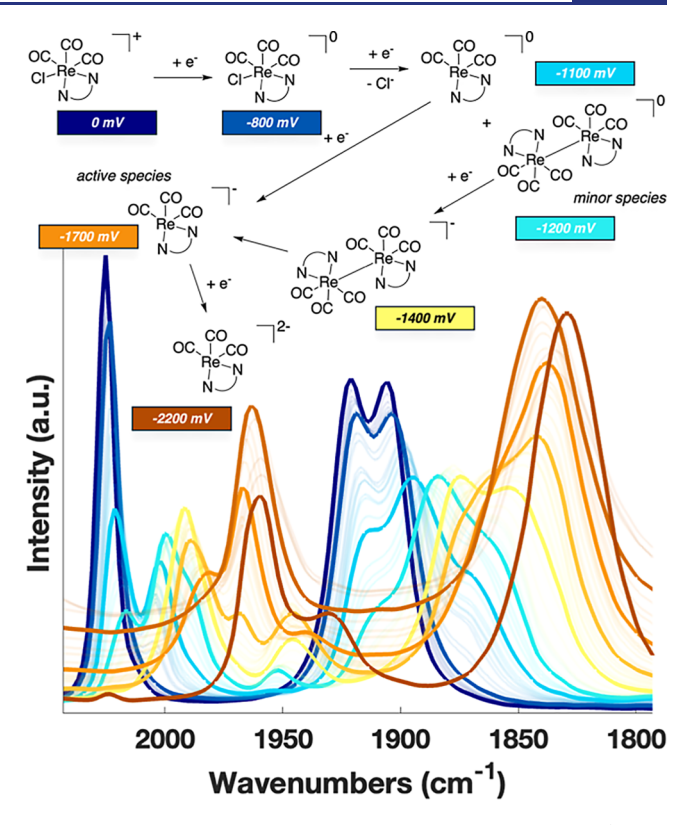


Figure 2. Homogeneous spectroelectrochemistry of [Re(phen-NHC)(CO)₃Cl][PF₆] in 100 mM TBAPF₆/ACN under inert conditions. The first and second spectral shifts (dark blue, light blue) are assigned as initially ligand-centered reduction processes. Upon loss of Cl-, dimerization at the rhenium center can occur (teal, diagnostic peak, 1952 cm⁻¹). The dimer may then undergo reduction (yellow, diagnostic peak, 1946 cm⁻¹) which cleaves to form the catalytically active species (orange) upon the addition of further electron density. An additional spectral shift (dark orange) can be observed under dynamic conditions. Potentials recorded vs an Ag quasi-reference electrode are included.

 cm^{-1} shift in $\nu(CO)_{symm}$ and the growth of a small band at 1952 cm⁻¹ characteristic of the Re⁰-Re⁰ dimer, the accumulation of which we attribute to intramolecular charge transfer allowed by the timescale of the technique (Figure 2). 47,42-45 At more reducing potentials, another spectral change occurs to afford what we believe is a further reduced dimer species, evidenced by a clear and rapid shift in the diagnostic dimer stretch to 1946 cm⁻¹. Such a species has been crystallized previously from a bipyridine-ligated analog.4 Additional applied potential results in reductive cleavage of the dimer and a ca. $27~{\rm cm}^{-1}$ shift in $\nu({\rm CO})_{\rm symm}$, corresponding to the formation of the catalytically active species. A final major spectral change in SEC likely corresponds to a formal rhenium reduction, as supported by DFT, and can be observed as a minor species by passing fresh solution of the analyte over a negatively charged electrode before the signal is convoluted by solvent decomposition.

Catalytic activity toward CO2 reduction was evaluated by CV and controlled-potential electrolysis (CPE). The observation of Faradaic features atop the catalytic curve is generally indicative of sluggish catalysis (Figure 1). Consistent with CV, electrolysis experiments using [Re(phen-NHC)(CO)₃Cl]⁺ as a homogeneous catalyst reveal poor performance toward CO2 reduction: Faradaic efficiency (FE) for CO production lies at just 28% (Table S12) where protons required for turnover are

Scheme 2. Proposed Mechanisms for Electrochemical Generation of Free Carbene From Aryl Imidazolium Cations^a

"Deprotonation mechanism adapted from ref 55. Available under a CC-BY 4.0 license. Copyright 2020 Amit et al. Reduction mechanism adapted with permission from ref 51. Copyright 2004 Royal Society of Chemistry.

abstracted from dry ACN. 1,40,46 This is not without precedent our group showed that the Re active site is very sensitive to the electronics of its polypyridyl ligand. Installing electron withdrawing ligands at the 4,4' position of Re(bpy-R)(CO)₃Cl devastated the FE for carbon products - from near unity with -tBu to only 18% FE_{CO} with -CN substituents under identical conditions. As we have seen, the additional aromaticity of the phen-NHC ligand leads to the localization (or rather, delocalization) of electrons across the ligand framework of [Re(phen-NHC)(CO)₃Cl]⁺, which appears to have the effect of reducing the overall FE for the desired catalytic reduction of CO₂. However, the poor performance of this catalyst in homogeneous solution is not necessarily a deterrent for studying immobilization effects. Recent work from our group showed that when a related group VII catalyst is immobilized on multiwalled carbon nanotubes, FE_{CO} jumps to ca. 92%, as compared to just 29% in solution.²⁸

Deposition of Molecular Catalyst on Au. With a baseline of accessible redox states of [Re(phen-NHC)-(CO)₃Cl]⁺ established in homogeneous solution, we sought to form a monolayer of the complex on a gold electrode surface using the -NHC functionality 47-50 Following recent work by our group,⁴⁸ a homoleptic bis(NHC)Au(I) cation of the rhenium complex, [Re(phen-NHC(CO)₃Cl)₂Au][PF₆], was synthesized, characterized, and evaluated by CV (see Figures S6-S7 and accompanying discussion). 48 Layers were prepared by soaking a clean Au substrate in a 0.1 mg/mL solution of the complex in ethanol for >12 h. Although $\nu(CO)$ stretches of the Re complex were observed by PM-IRRAS following deposition, these features repeatedly disappeared after modest voltammetric interrogation under Ar and CO₂ (Figure S8). A fourth reduction wave is distinctly absent from CV of Re(phen-NHC)(CO)₃Cl)₂Au][PF₆] (Figure S7). Based on this, we initially believed that this feature of [Re(phen-NHC)(CO)₃Cl]⁺ may correspond to the reduction of the aryl imidazolium moiety, resulting in the free carbene.^{51,52} We theorized that a more stable monolayer could be formed by direct attachment of the molecule to an Au working electrode via in situ electrochemical generation of the carbene species from the imidazolium salt and concomitant deposition onto a gold working electrode. 51-54 While additional electronic characterization of [Re(phen-NHC)(CO)₃Cl]⁺ showed that the fourth redox feature in CV was not due to a localized reduction of the imidazolium (vide supra), we did find that

slow (25 mV/s), repeated electrochemical cycling to the corresponding reduction potential (ca. -2.2 V vs Fc/Fc⁺ in TBAPF₆/ACN) resulted in monolayers exhibiting defined vibrational modes characteristic of the Re(CO)₃ moiety by PM-IRRAS and Faradaic features in CV (*vide infra*).

The electrochemical deposition of NHCs on Au using controlled potential electrolysis at −1 V vs an Ag/AgBr pseudoreference electrode in wet (50 mM H₂O) acetonitrile has been reported previously, the proposed mechanism of which entails reduction of H2O to form OH ions at the electrochemical interface, which subsequently deprotonate the imidazolium moiety to form the free carbene (Scheme 2).55 In our hands, we did not observe current enhancement corresponding to water reduction at such low concentrations until potentials negative of -2.2 V vs Fc/Fc⁺ in acetonitrile (See Figure S11 and accompanying discussion). Interestingly, we find that [Re(phen-NHC)(CO)₃Cl]⁺ can be deposited on Au via controlled potential electrolysis at much less negative potentials under anhydrous conditions (as characterized by PM-IRRAS, Figure S12). Based on these findings, experiments were performed to elucidate the mechanism of deposition. In an N₂ filled glovebox, [Re(phen-NHC)(CO)₃Cl]⁺ was separately exposed to tetrabutylammonium hydroxide and a chemical reductant, potassium graphite. The resulting solutions were characterized by IR spectroscopy, and clean Au slides were subsequently immersed in each solution. In both cases, diagnostic CO modes are visible in the resulting PM-IRRAS spectra, indicating deposition of the complex (Figure S15). Of great interest is a ca. 2 cm⁻¹ red shift in $\nu(CO)$ of the molecule in solution-state IR upon exposure to both base and chemical reductant (Figure 3). This shift is also reflected in the spectroelectrochemistry of the molecule, and is accompanied by the loss of a broad feature at ca. 3080 cm⁻¹ that we assign as the ⁺C-H stretch of the imidazolium cation (see Figures S9 and S16, Table S5).⁵⁶ Consequently, this shift corresponds to the apparent formation of the carbene complex which can subsequently bind to gold.

Direct electrochemical reduction of the imidazolium cation is likely to proceed through a radical mechanism, reacting with either itself or solvent to release hydrogen gas and generate the free carbene (Scheme 2).^{51,52} DFT calculations of [Re(phen-NHC)(CO)₃Cl]⁺ were performed to evaluate the energetics of this process, which, unsurprisingly, is strongly endergonic for the unreduced cationic species: +2.77 eV (63.88 kcal/mol).

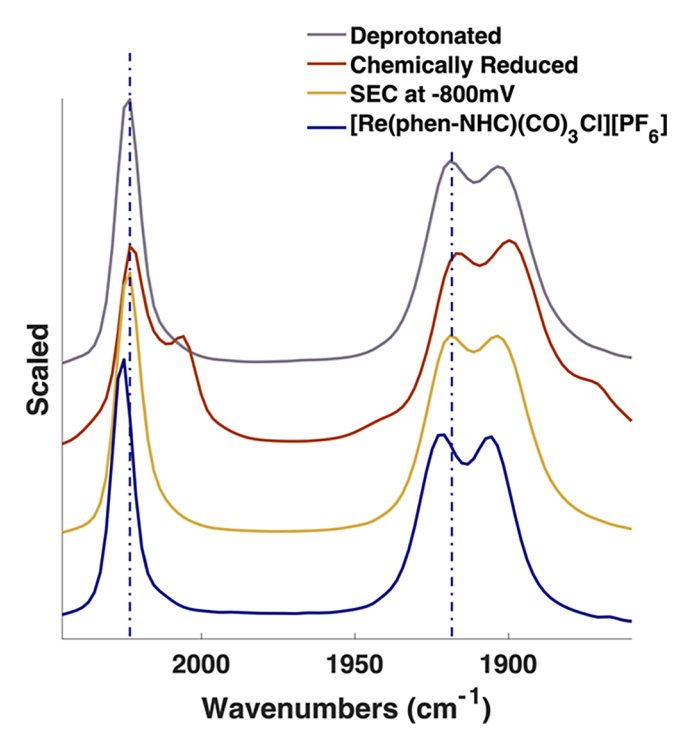


Figure 3. Solution-state IR in ACN of signature CO stretches of $[Re(phen-NHC)(CO)_3Cl]^+$ (blue) after exposure to tetrabutylammonium hydroxide (gray), potassium graphite (red), and under negative bias during spectroelectrochemical measurements (yellow). Peak values are reported in Table S7.

Upon reduction of the complex, however, hydrogen release becomes thermodynamically accessible, just +0.08 eV (1.8 kcal/mol) uphill after the first redox event and +0.10 eV (2.3 kcal/mol) after the second. As additional electron density is added to the molecule, the process becomes favorable: -0.55eV (-12.68 kcal/mol) after the third reduction, and -0.61 eV(-14.07 kcal/mol) after the fourth reduction of the complex. Spectroelectrochemical evidence of conversion to the carbene species and irreversibility of the first reduction feature at very slow scan rates in CV (Figure S3) suggest that the rate of carbene formation is dominated by the chemical hydrogen atom transfer step. Taken together with experimental results, these computational analyses support that electrochemical generation of the free carbene begins to occur after the first reduction of [Re(phen-NHC)(CO)₃Cl]⁺ and prevails at higher reducing potentials. Therefore, we believe that the reduction mechanism of [Re(phen-NHC)(CO)₃Cl]⁺ depicted in Scheme 2 dominates during our deposition procedures.

In addition to our original grafting technique, wherein slow (25 mV/s) electrochemical cycling was performed to ca. -2.2 V vs Fc/Fc⁺ (the fourth reduction potential of the molecule), we investigated single-potential electrolysis depositions and cycling to less negative potentials using the redox features of [Re(phen-NHC)(CO)₃Cl]⁺ as an internal reference in TBAPF₆/ACN. PM-IRRAS of an Au slide subjected to single-potential electrolysis depositions reveals a "goldilocks" potential zone for effective deposition, where applied potentials of ca. -1.7 and ca. -2.0 V vs Fc/Fc⁺ (corresponding to the second and third reduction potentials of the complex) result in the most intense ν (CO) bands (Figure S12). Notably, electrolysis depositions at the potential of the fourth reduction resulted in low PM-IRRAS intensity. Based on this finding, we also tested electrochemical cycling to the potential of the

second reduction feature (ca. -1.7 V vs Fc/Fc⁺), which produced visible $\nu(CO)$ modes in PM-IRRAS spectra (Figure S14). Cycling to, and electrolysis at −1.7 V vs Fc/Fc⁺ produced layers with similar stability properties under successive 60 s controlled-potential electrolysis experiments (Table S6), with a slightly more negative catalytic onset potential apparent for electrolysis depositions (Figure S19). Of the deposition methods tested, cycling to the fourth reduction potential allowed the most electroactive complex to be deposited (as determined by integration of redox features in CV, Figure S19). We theorize that grafting through electrochemical cycling benefits from a combination of increased time spent at reducing potentials and increased thermodynamic driving force for hydrogen atom donation by the imidazolium cation. Additionally, cycling to very negative potentials may allow molecules deposited in an unfavorable configuration for electron transfer to reconfigure or strip, leaving a vacancy for another molecule to rebind on the next cycle. For consistency, we discuss monolayers which were deposited through slow cycling to -2.2 V vs Fc/Fc⁺ and refer to the gold-bound system as an Electrochemically-Assembled Monolayer (ELAM) below. Surface coverage was evaluated via cyclic voltammetry and ICP-MS. Through both methods, monolayer coverage was determined to be on the order of 10¹³ molecules/cm² when calculated using the geometric surface area of Au electrodes. Though on the low end, this value is in agreement with established monolayer loadings⁵⁷ and with the crystal packing density of [Re(phen-NHC)(CO)₃Cl]⁺, and is therefore attributed to the spatially demanding -Bz groups attached to the phen-NHC framework. It is important to note, however, that these values can also be highly dependent on the electroactive surface area of each Au substrate. Selected values and additional discussion are reported in the Supporting Information (Tables S9 and 10).

Characterization of Immobilized Catalyst. Vibrational spectroscopy of the CO stretching region of Re(phen-NHC)(CO)₃X ELAMs on 1 cm² Au slides is presented in Figure 4 (see Figure S25 for full PM-IRRAS spectrum). Comparison of the $\nu(CO)$ spectral features of the ELAM with the FT-IR spectrum of [Re(phen-NHC)(CO)₃Cl]⁺ in acetonitrile reveals a Gaussian peak distribution characteristic of inhomogeneous broadening, supporting the covalent binding of the heterogenized Re(phen-NHC)(CO)₃X to the gold surface.⁵⁸ To obtain a more detailed understanding, DFT calculations of the vibrational modes of an Au-bound Re(phen-NHC)(CO)₃Cl were performed using a cluster-based model (see Supporting Information), following our previous studies on the surface orientation of rhenium tricarbonyl catalysts.⁵⁹ PM-IRRAS selection rules dictate that peak intensity depends on the angle between the transition dipole moment of the vibrational modes and surface normal, 60 therefore the relative intensities of the $\nu(CO)$ features provide information on the averaged relative orientation of the complex on the surface. A fit of the experimental PM-IRRAS spectrum results in three peaks with amplitudes of 6.18, 5.98 (asymmetric modes), and 7.92 au (symmetric mode) (see Table S19), which, upon comparison with the computational PM-IRRAS intensities, suggests that the orientation of the rhenium carbonyl moiety is canted 50-60° relative to the Au electrode surface.

Cyclic voltammetry under Ar of Re(phen-NHC)(CO)₃X ELAMs formed on 3 mm diameter Au electrodes exhibit redox features particularly visible with increasing scan rate. The scan rate dependence of the peak current was investigated to

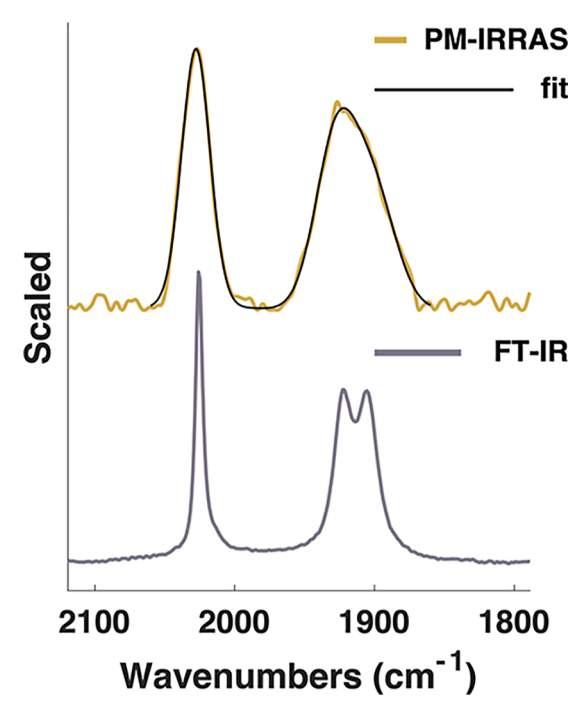


Figure 4. PM-IRRAS spectrum of signature $\nu(CO)$ stretches of heterogenized Re(phen-NHC)(CO)₃X and Levenberg–Marquardt fit (top) compared to solution-state FT-IR spectrum of [Re(phen-NHC)(CO)₃CI]⁺ in acetonitrile (bottom). Band shape analysis of each $\nu(CO)$ stretch was over 90% Gaussian in character.

determine the species observed was surface-bound (Figure 5). A linear dependence of the major peak current vs scan rate was found, reflective of a redox process that is not diffusion-limited, i.e., the analyte is confined to the electrode. The reduction features of the heterogenized molecule are less distinct as compared to its response in solution, making the assignment of

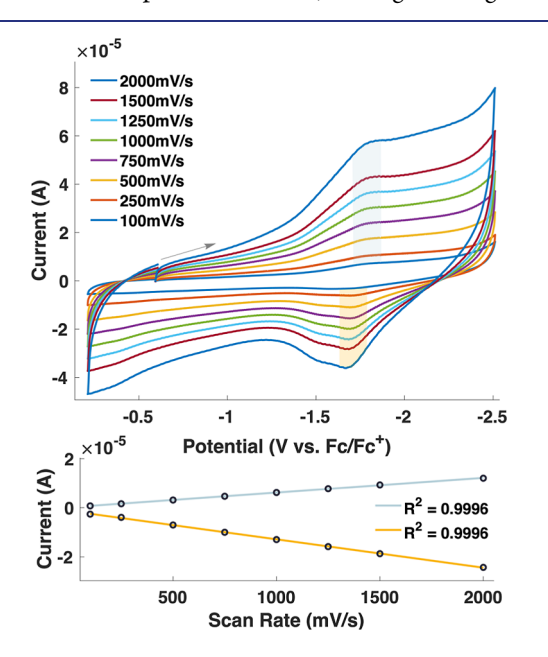


Figure 5. Scan rate dependence of reduction features of heterogenized Re(phen-NHC)(CO) $_3$ X (above) in 100 mM TBAPF $_6$ /ACN under Ar. The forward and reverse peak current varies linearly with scan rate (below), indicative that the redox active species observed is bound to the electrode.

specific processes challenging. We suspect that the hybridization of the molecular species with the biased electrode may affect the electronic structure and orientation of the bound molecule, and by effect, change the character of the observed redox features relative to the species in solution. These electronic effects are under investigation and will be the subject of a future work. The peak-to-peak separation of the major redox features under Ar is nonzero (average $\Delta E_p = 69$ mV). Electrode adsorbed redox-active complexes theoretically do not exhibit peak-to-peak separation under purely reversible conditions, as the potential for the couple should not be limited by diffusion. This deviation from ideality has been explained in detail elsewhere. 62 Surface defects of polycrystalline Au, 63-65 quasireversibility of closely spaced redox features, and lateral interactions between immobilized molecules (e.g., dimerization) are all likely candidates to cause the observed broadening and peak shift. 57,62,66

Activity toward CO₂ Reduction. Significant catalytic current is observed coinciding with the reduction features of Re(phen-NHC)(CO)₃X ELAMs under an atmosphere of CO₂ (Figure 6). The character of the wave is distinct from both the homogeneous species and from bare Au. The potential of catalytic onset is positive than that of the bare electrode in dry electrolyte. To compare the activity of the homogeneous and heterogenized species, the observed rate of catalysis was calculated using the i_{cat}/i_p method^{1,67} assuming all charge is accounted for by $n = 2e^-$ reduction products. Based on cyclic

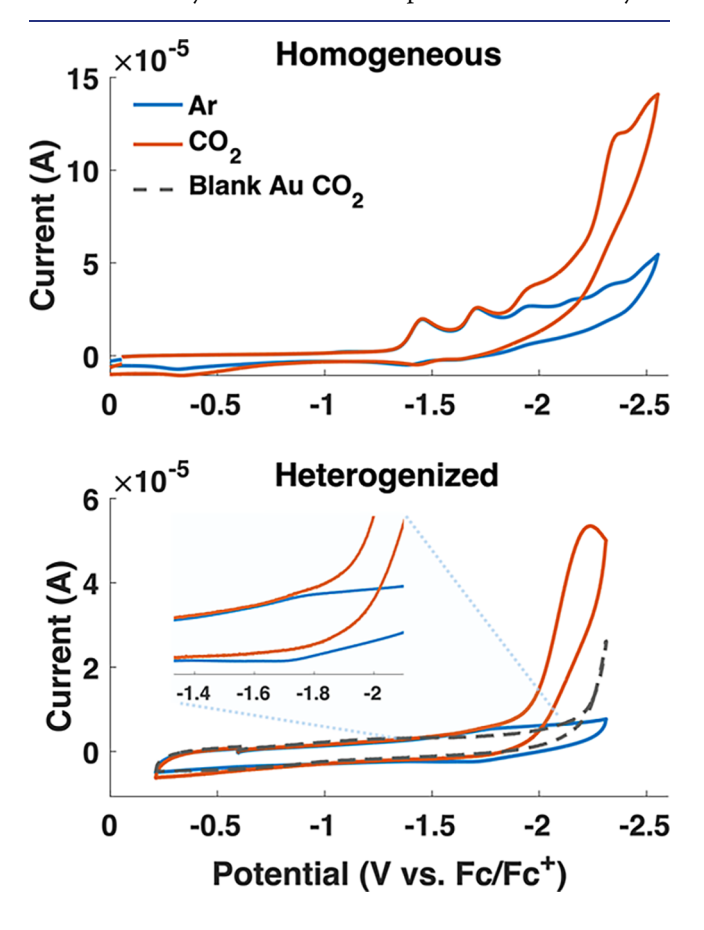


Figure 6. Catalytic current enhancement under CO_2 by 1 mM $[Re(phen-NHC)(CO)_3Cl]^+$ (above) vs $Re(Phen-NHC)(CO)_3X$ heterogenized on Au (below) in 100 mM TBAPF₆/ACN. The onset potential of catalysis for homogeneous and heterogeneous species is over 200 mV positive than that of blank Au in dry ACN.

voltammetry alone, the observed rate of the homogeneous catalyst was determined to be 4 s⁻¹, while the heterogenized system is faster by a factor of over 200 (947 s⁻¹) (Table S11). We recognize that this equation is only correctly applicable to ideal S-shaped catalytic curves. 67-69 In our analysis, we sought to compare the relative activity of the homogeneous and heterogenized species rather than an intrinsic rate of catalysis and encourage the reader to interpret these values accordingly. Gaseous product quantification derived from controlled potential electrolysis experiments under 1 atm CO₂ confirms product formation and results in a more practical value for selectivity: 64% FE_{CO} at -2200 mV vs Fc/Fc⁺ for the ELAM in dry ACN. Activity toward CO₂ reduction of the heterogenized system surpasses both the homogeneous compound (FE_{CO} = 28%) and bare Au (FE $_{CO}$ = 23%), in general agreement with CV (Table S12). We attribute the apparent improvement in performance over the homogeneous species to two phenomena associated with direct conjugation to the electrode: first, that catalyst turnover is limited only by diffusion of the substrate rather than both substrate and catalyst, and second, because electron transfer may proceed with low reorganization energy between the catalyst and the electrode through the carbene-Au bond.

Stability of the Immobilized Catalyst. To investigate the stability of the heterogenized species, an initial survey of high cathodic bias electrolysis experiments was performed using an ELAM on a 3 mm diameter Au electrode. Potentials of -2.1 and -2.3 V vs Fc/Fc⁺ were applied for 15 s each, for a total of four experiments under Ar and CO₂ (Figure S21). CV scans were taken before and after each corresponding electrolysis experiment and are reported in Figure S22. Notably, a sharp reductive stripping peak like those observed for thiol-based monolayers does not appear. 64 While a moderate current decrease in Faradaic features and the catalytic wave is observed, signals arising from the surfacebound species are still present after electrolysis. To confirm the presence of Re(Phen-NHC)(CO)₃X on Au under such conditions, a comparable stability study was performed on a 1 cm² Au slide, which was analyzed via PM-IRRAS before and after deposition and each successive electrolysis experiment. Small deleterious effects were observed with progressive scans negative of −2 V vs Fc/Fc⁺ and CPE under CO₂ in both dry and wet ACN (Figure S23). However, even after several CPE experiments under catalytic conditions, signature $\nu(CO)$ stretches remain visible via PM-IRRAS (Figure S25).

The stability of the monolayer was also examined through XPS and PM-IRRAS analysis together with a product quantification experiment on a 1 cm² Au slide (Figure 7, Figure S26). After 42 mC of charge was passed under catalytic conditions (ca. 2 min for the monolayer analyzed, Figure S24), signal arising from Re(phen-NHC)(CO)₃X persisted in the PM-IRRAS spectrum, and XPS analysis indicated that ca. 41% Re was retained as measured by the area of the Re 4f peak. Likely causes for the decrease in signal observed include stripping of carbene-bound Au adatoms, ⁷⁰ catalyst deactivation (i.e., demetalation/complex degradation - after all, molecular catalysts have a limited turnover number), or simple cathodic stripping of the NHC-bound molecule. The latter is to be expected under the severe conditions experienced at the electrode/electrolyte interface at high bias. Interfacial electric fields can be as large as 10^9 V/m, depending on the character of the monolayer and electrolyte. 71,72 Furthermore, under cathodic bias, reduced immobilized species are held in close

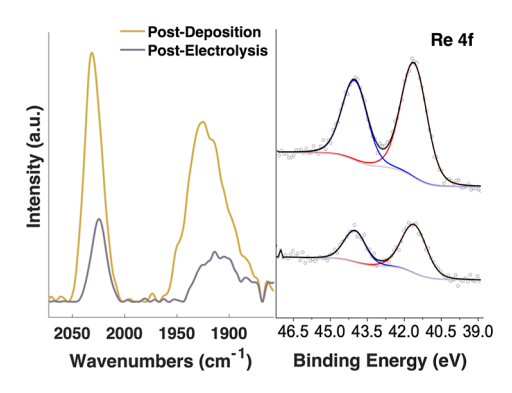


Figure 7. PM-IRRAS spectra of $\nu(CO)$ bands of the heterogenized catalyst before and after product quantification electrolysis under CO_2 at -2.2~V vs Fc/Fc⁺ (Left Panel). XP spectra of Re 4f before (top) and after (bottom) the catalytic measurement (Right Panel). The colored curves represent the fitted peaks corresponding to the Re 4f $_{7/2}$ (red) and 4f $_{5/2}$ components (blue).

proximity to a negatively charged electrode, the electrostatic repulsion of which may be extreme on the molecular scale.

The potential window of stability of NHC-based monolayers on gold for industrially relevant electrochemical applications has been studied previously. One group used SERS to monitor stretches of commonly studied benzimidazole-based NHCs on roughened gold under continuous voltammetric cycling up to 67.7 h, suggesting a cathodic potential window of stability for this species out to -1 V vs Ag/AgCl (between -1.41 and -1.45 V vs Fc/Fc⁺) over long periods of use.^{73,74} Due to the native activity of gold toward CO2 reduction, applications using the NHC-based attachment to gold described herein are best found in catalytic transformations requiring a more moderate bias and where substrate does not interfere. Still, the linker design and deposition method presented may enable deeper cathodic excursions in in situ spectroelectrochemical investigations. Electrochemical and infrared signals from this ELAM endure voltammetric scans negative of -2 V vs Fc/Fc⁺ and through sustained catalysis, providing a promising platform to study electric field and immobilization effects on covalently bound molecular species.

CONCLUSIONS

We report an electrochemically grafted monolayer of a molecular rhenium CO2 reduction catalyst on gold electrodes. Electrochemical cycling in a solution of [Re(phen-NHC)-(CO)₃Cl]⁺ generates the corresponding free carbene in situ, depositing the species on working Au electrodes. The addition of the Re(CO)₃ moiety to the polypyridyl NHC-linker provides a meaningful spectroscopic handle to diagnose the mechanism of deposition and attachment to Au. Signature CO stretches observed in PM-IRRAS spectra reveal inhomogeneous broadening characteristic of a surface-bound species at a 50-60° tilt angle, and Faradaic features of the heterogenized molecule and catalytic current under CO₂ are visible via CV. Compared to the homogeneous catalyst, the immobilized species exhibits greater selectivity for CO2 reduction products and a faster rate of catalysis via CV. The NHC-based monolayer demonstrates durability in organic solvent through repeated scans beyond -2 V vs Fc/Fc⁺ and catalytic electrolysis, with the goal of enabling spectroelectrochemical investigations of electrode conjugation and interfacial electric field effects on polypyridyl-ligated molecular species. Furthermore, the method of immobilization presented here may

be extended to other materials (e.g., Cu, Pt, Ag) allowing for a convenient electrode modification protocol using carbene-based attachments from bench stable imidazolium precursors.

ASSOCIATED CONTENT

Data Availability Statement

Crystallographic data for $[Re(phen-NHC)(CO)_3Cl][PF_6]$ has been deposited at the CCDC under no. 2395549.

Supporting Information

The Supporting Information is available free of charge at https://pubs.acs.org/doi/10.1021/jacs.5c11267.

Experimental details, synthetic methods and characterization of all compounds (¹H NMR, IR, ESI-MS), crystallographic data, additional electrochemical data (CV, CPE) and spectroscopic data (IR, PM-IRRAS), equations for calculation of overpotential and TOF, computational details (PDF)

Accession Codes

Deposition Number 2395549 contains the supplementary crystallographic data for this paper. These data can be obtained free of charge via the joint Cambridge Crystallographic Data Centre (CCDC) and Fachinformationszentrum Karlsruhe Access Structures service.

AUTHOR INFORMATION

Corresponding Authors

Victor S. Batista — Department of Chemistry and Energy Sciences Institute, Yale University, New Haven, Connecticut 06520, United States; orcid.org/0000-0002-3262-1237; Email: victor.batista@yale.edu

Clifford P. Kubiak — Department of Chemistry and Biochemistry, University of California, San Diego, La Jolla, California 92093, United States; orcid.org/0000-0003-2186-488X; Email: ckubiak@ucsd.edu

Authors

Lydia R. Weddle — Department of Chemistry and Biochemistry, University of California, San Diego, La Jolla, California 92093, United States; orcid.org/0009-0000-7489-0585

Jan Paul Menzel – Department of Chemistry and Energy Sciences Institute, Yale University, New Haven, Connecticut 06520, United States; orcid.org/0000-0002-1312-5000

Pablo E. Videla — Department of Chemistry and Energy Sciences Institute, Yale University, New Haven, Connecticut 06520, United States; Oorcid.org/0000-0003-0742-0342

Emile E. DeLuca — Department of Chemistry and Biochemistry, University of California, San Diego, La Jolla, California 92093, United States; orcid.org/0000-0002-9783-5922

Hao Fan Su – Department of Chemistry and Biochemistry, University of California, San Diego, La Jolla, California 92093, United States

Hao Chen – Pulse Institute, SLAC National AcceleratorLaboratory, Menlo Park, California 94025, United States

Joseph M. Palasz – Department of Chemistry and Biochemistry, University of California, San Diego, La Jolla, California 92093, United States

James M. Taylor – Department of Chemistry and Biochemistry, University of California, San Diego, La Jolla, California 92093, United States Zhuoran Long — Department of Chemistry and Energy Sciences Institute, Yale University, New Haven, Connecticut 06520, United States; oorcid.org/0000-0002-2957-9568

Complete contact information is available at: https://pubs.acs.org/10.1021/jacs.5c11267

Notes

The authors declare no competing financial interest.

ACKNOWLEDGMENTS

The authors acknowledge Dr. Jinhui Meng for preliminary spectroscopic results, Dr. Thomas Chan for fabrication of gold slides, and Ritchie Hernandez for preliminary SCXRD results. We also thank the UCSD Molecular Mass Spectrometry Facility and CAICE Environmental and Complex Analysis Laboratory for sample analysis. This material is based upon work supported by NSF (CHE 2452001, CHE-1853908, and CHE-2153757) and by the National Science Foundation Graduate Research Fellowship Program under Grant No. DGE-2038238. Any opinions, findings, and conclusions or recommendations expressed in this material are those of the author(s) and do not necessarily reflect the views of the National Science Foundation.

REFERENCES

- (1) Clark, M. L.; Cheung, P. L.; Lessio, M.; Carter, E. A.; Kubiak, C. P. Kinetic and Mechanistic Effects of Bipyridine (bpy) Substituent, Labile Ligand, and Brønsted Acid on Electrocatalytic CO₂ Reduction by Re(bpy) Complexes. *ACS Catal.* **2018**, *8* (3), 2021–2029.
- (2) Sampson, M.; Froehlich, J.; Smieja, J.; Benson, E.; Sharp, I.; Kubiak, C. Direct observation of the reduction of carbon dioxide by rhenium bipyridine catalysts. *Energy Environ. Sci.* **2013**, *6* (12), 3748–3755.
- (3) Benson, E. E.; Grice, K. A.; Smieja, J. M.; Kubiak, C. P. Structural and spectroscopic studies of reduced Re(bpy-R)(CO)(3) (-1) species relevant to CO2 reduction. *Polyhedron* **2013**, *58*, 229–234.
- (4) Benson, E. E.; Kubiak, C. P. Structural investigations into the deactivation pathway of the CO2 reduction electrocatalyst Re(bpy)-(CO)3Cl. Chem. Commun. 2012, 48 (59), 7374–7376.
- (5) Benson, E. E.; Sampson, M. D.; Grice, K. A.; Smieja, J. M.; Froehlich, J. D.; Friebel, D.; Keith, J. A.; Carter, E. A.; Nilsson, A.; Kubiak, C. P. The Electronic States of Rhenium Bipyridyl Electrocatalysts for CO2 Reduction as Revealed by X-ray Absorption Spectroscopy and Computational Quantum Chemistry. *Angew. Chem., Int. Ed.* 2013, 52 (18), 4841–4844.
- (6) Barrett, J. A.; Miller, C. J.; Kubiak, C. P. Electrochemical Reduction of CO2 Using Group VII Metal Catalysts. *Trends Chem.* **2021**, *3* (3), 176–187.
- (7) Smieja, J. M.; Kubiak, C. P. Re(bipy-tBu)(CO)3Cl-improved Catalytic Activity for Reduction of Carbon Dioxide: IR-Spectroelectrochemical and Mechanistic Studies. *Inorg. Chem.* **2010**, 49 (20), 9283–9289.
- (8) Sampson, M. D.; Froehlich, J. D.; Smieja, J. M.; Benson, E. E.; Sharp, I. D.; Kubiak, C. P. Direct observation of the reduction of carbon dioxide by rhenium bipyridine catalysts. *Energy Environ. Sci.* **2013**, *6* (12), 3748–3755.
- (9) Chabolla, S. A.; Dellamary, E. A.; Machan, C. W.; Tezcan, F. A.; Kubiak, C. P. Combined steric and electronic effects of positional substitution on dimethyl-bipyridine rhenium(I)tricarbonyl electrocatalysts for the reduction of CO2. *Inorg. Chim. Acta* **2014**, 422, 109–113.
- (10) Tada, M.; Iwasawa, Y. Advanced design of catalytically active reaction space at surfaces for selective catalysis. *Coord. Chem. Rev.* **2007**, 251 (21), 2702–2716.

- (11) Kuhl, K. P.; Cave, E. R.; Abram, D. N.; Jaramillo, T. F. New insights into the electrochemical reduction of carbon dioxide on metallic copper surfaces. *Energy Environ. Sci.* **2012**, *5* (5), 7050–7059.
- (12) Nitopi, S.; Bertheussen, E.; Scott, S. B.; Liu, X.; Engstfeld, A. K.; Horch, S.; Seger, B.; Stephens, I. E. L.; Chan, K.; Hahn, C.; et al. Progress and Perspectives of Electrochemical CO2 Reduction on Copper in Aqueous Electrolyte. *Chem. Rev.* **2019**, *119* (12), 7610–7672.
- (13) Huffman, B. L.; Bein, G. P.; Atallah, H.; Donley, C. L.; Alameh, R. T.; Wheeler, J. P.; Durand, N.; Harvey, A. K.; Kessinger, M. C.; Chen, C. Y.; et al. Surface Immobilization of a Re(I) Tricarbonyl Phenanthroline Complex to Si(111) through Sonochemical Hydrosilylation. ACS Appl. Mater. Interfaces 2023, 15 (1), 984–996.
- (14) Jia, X.; Nedzbala, H. S.; Bottum, S. R.; Cahoon, J. F.; Concepcion, J. J.; Donley, C. L.; Gang, A.; Han, Q.; Hazari, N.; Kessinger, M. C.; et al. Synthesis and Surface Attachment of Molecular Re(I) Complexes Supported by Functionalized Bipyridyl Ligands. *Inorg. Chem.* 2023, 62 (5), 2359–2375.
- (15) Bullock, R. M.; Das, A. K.; Appel, A. M. Surface Immobilization of Molecular Electrocatalysts for Energy Conversion. *Chemistry* **2017**, 23 (32), 7626–7641.
- (16) Choate, J. C.; Silva, I., Jr.; Hsu, P. C.; Tran, K.; Marinescu, S. C. The Positional Effect of an Immobilized Re Tricarbonyl Catalyst for CO(2) Reduction. ACS Appl. Mater. Interfaces **2024**, 16 (38), 50534–50549.
- (17) Zhanaidarova, A.; Ostericher, A. L.; Miller, C. J.; Jones, S. C.; Kubiak, C. P. Selective Reduction of CO2 to CO by a Molecular Re(ethynyl-bpy)(CO)3Cl Catalyst and Attachment to Carbon Electrode Surfaces. *Organometallics* **2019**, *38* (6), 1204–1207.
- (18) Sun, C.; Rotundo, L.; Garino, C.; Nencini, L.; Yoon, S. S.; Gobetto, R.; Nervi, C. Electrochemical CO2 Reduction at Glassy Carbon Electrodes Functionalized by MnI and ReI Organometallic Complexes. *ChemPhysChem* **2017**, *18* (22), 3219–3229.
- (19) Willkomm, J.; Bertin, E.; Atwa, M.; Lin, J.-B.; Birss, V.; Piers, W. E. Grafting of a Molecular Rhenium CO2 Reduction Catalyst onto Colloid-Imprinted Carbon. *ACS Appl. Energy Mater.* **2019**, 2 (4), 2414–2418.
- (20) Jackson, M. N.; Surendranath, Y. Molecular Control of Heterogeneous Electrocatalysis through Graphite Conjugation. *Acc. Chem. Res.* **2019**, 52 (12), 3432–3441.
- (21) Oh, S.; Gallagher, J. R.; Miller, J. T.; Surendranath, Y. Graphite-Conjugated Rhenium Catalysts for Carbon Dioxide Reduction. *J. Am. Chem. Soc.* **2016**, *138* (6), 1820–1823.
- (22) Jackson, M. N.; Oh, S.; Kaminsky, C. J.; Chu, S. B.; Zhang, G.; Miller, J. T.; Surendranath, Y. Strong Electronic Coupling of Molecular Sites to Graphitic Electrodes via Pyrazine Conjugation. *J. Am. Chem. Soc.* **2018**, *140* (3), 1004–1010.
- (23) Jackson, M. N.; Kaminsky, C. J.; Oh, S.; Melville, J. F.; Surendranath, Y. Graphite Conjugation Eliminates Redox Intermediates in Molecular Electrocatalysis. *J. Am. Chem. Soc.* **2019**, *141* (36), 14160–14167
- (24) Kaminsky, C. J.; Wright, J.; Surendranath, Y. Graphite-Conjugation Enhances Porphyrin Electrocatalysis. *ACS Catal.* **2019**, 9 (4), 3667–3671.
- (25) Fukushima, T.; Drisdell, W.; Yano, J.; Surendranath, Y. Graphite-Conjugated Pyrazines as Molecularly Tunable Heterogeneous Electrocatalysts. *J. Am. Chem. Soc.* **2015**, *137* (34), 10926–10929.
- (26) Zhanaidarova, A.; Jones, S. C.; Despagnet-Ayoub, E.; Pimentel, B. R.; Kubiak, C. P. Re(tBu-bpy)(CO)3Cl Supported on Multi-Walled Carbon Nanotubes Selectively Reduces CO2 in Water. *J. Am. Chem. Soc.* **2019**, *141* (43), 17270–17277.
- (27) DeLuca, E. E.; Chan, T.; Taylor, J. M.; Lee, B.; Prabhakar, R. R.; Kubiak, C. P. Steric Effects on CO2 Reduction with Substituted Mn(bpy)(CO)3X-Type Catalysts on Multiwalled Carbon Nanotubes Reveal Critical Mechanistic Details. ACS Catal. 2024, 14 (3), 2071–2083
- (28) Lee, A. J.; DeLuca, E. E.; Kelly, E. B.; Taylor, J. M.; Weddle, L. R.; Chen, H.; Park, C.; Loeb, C. K.; Chan, T.; Kubiak, C. P.

- Cambered Bipyridyl Ligand with Extended Aryl System Enables Electrochemical Reduction of Carbon Dioxide and Bicarbonate by Mn(bpy)(CO)(3)Br-type Catalyst Immobilized on Carbon Nanotubes. J. Am. Chem. Soc. 2025, 147 (9), 7411–7422.
- (29) Bhattacharyya, D.; Videla, P.; Cattaneo, M.; Batista, V.; Lian, T.; Kubiak, C. Vibrational Stark shift spectroscopy of catalysts under the influence of electric fields at electrode-solution interfaces. *Chem. Sci.* **2021**, *12* (30), 10131–10149.
- (30) Lake, W. R.; Meng, J.; Dawlaty, J. M.; Lian, T.; Hammes-Schiffer, S. Electro-inductive Effect Dominates Vibrational Frequency Shifts of Conjugated Probes on Gold Electrodes. *J. Am. Chem. Soc.* **2023**, *145* (41), 22548–22554.
- (31) Clark, M. L.; Ge, A.; Videla, P. E.; Rudshteyn, B.; Miller, C. J.; Song, J.; Batista, V. S.; Lian, T.; Kubiak, C. P. CO2 Reduction Catalysts on Gold Electrode Surfaces Influenced by Large Electric Fields. J. Am. Chem. Soc. 2018, 140 (50), 17643–17655.
- (32) Long, Z.; Meng, J.; Weddle, L. R.; Videla, P. E.; Menzel, J. P.; Cabral, D. G. A.; Liu, J.; Qiu, T.; Palasz, J. M.; Bhattacharyya, D.; et al. The Impact of Electric Fields on Processes at Electrode Interfaces. *Chem. Rev.* **2025**, *125* (3), 1604–1628.
- (33) Sarkar, S.; Patrow, J. G.; Voegtle, M. J.; Pennathur, A. K.; Dawlaty, J. M. Electrodes as Polarizing Functional Groups: Correlation between Hammett Parameters and Electrochemical Polarization. *J. Phys. Chem. C* **2019**, 123 (8), 4926–4937.
- (34) Heo, J.; Ahn, H.; Won, J.; Son, J. G.; Shon, H. K.; Lee, T. G.; Han, S. W.; Baik, M.-H. Electro-inductive effect: Electrodes as functional groups with tunable electronic properties. *Science* **2020**, 370 (6513), 214–219.
- (35) Wright, D.; Lin, Q.; Berta, D.; Földes, T.; Wagner, A.; Griffiths, J.; Readman, C.; Rosta, E.; Reisner, E.; Baumberg, J. J. Mechanistic study of an immobilized molecular electrocatalyst by in situ gapplasmon-assisted spectro-electrochemistry. *Nat. Catal.* **2021**, *4* (2), 157–163.
- (36) Crudden, C. M.; Horton, J. H.; Ebralidze, I. I.; Zenkina, O. V.; McLean, A. B.; Drevniok, B.; She, Z.; Kraatz, H.-B.; Mosey, N. J.; Seki, T.; et al. Ultra stable self-assembled monolayers of N-heterocyclic carbenes on gold. *Nat. Chem.* **2014**, *6* (5), 409–414.
- (37) Naithani, S.; Goswami, T.; Thetiot, F.; Kumar, S. Imidazo [4,5-f][1,10]phenanthroline based luminescent probes for anion recognition: Recent achievements and challenges. *Coord. Chem. Rev.* **2023**, 475. 214894.
- (38) Neyhouse, B. J.; White, T. A. Modifying the steric and electronic character within Re(I)-phenanthroline complexes for electrocatalytic CO2 reduction. *Inorg. Chim. Acta* **2018**, *479*, 49–57.
- (39) Smieja, J. M.; Benson, E. E.; Kumar, B.; Grice, K. A.; Seu, C. S.; Miller, A. J. M.; Mayer, J. M.; Kubiak, C. P. Kinetic and structural studies, origins of selectivity, and interfacial charge transfer in the artificial photosynthesis of CO. *Proc. Natl. Acad. Sci. U. S. A.* **2012**, 109 (39), 15646–15650.
- (40) Smieja, J. M.; Sampson, M. D.; Grice, K. A.; Benson, E. E.; Froehlich, J. D.; Kubiak, C. P. Manganese as a Substitute for Rhenium in CO₂ Reduction Catalysts: The Importance of Acids. *Inorg. Chem.* **2013**, 52 (5), 2484–2491.
- (41) Riplinger, C.; Sampson, M. D.; Ritzmann, A. M.; Kubiak, C. P.; Carter, E. A. Mechanistic Contrasts between Manganese and Rhenium Bipyridine Electrocatalysts for the Reduction of Carbon Dioxide. *J. Am. Chem. Soc.* **2014**, *136* (46), 16285–16298.
- (42) Machan, C. W.; Sampson, M. D.; Chabolla, S. A.; Dang, T.; Kubiak, C. P. Developing a Mechanistic Understanding of Molecular Electrocatalysts for CO₂ Reduction using Infrared Spectroelectrochemistry. *Organometallics* **2014**, 33 (18), 4550–4559.
- (43) Fujita, E.; Muckerman, J. T. Why Is Re–Re Bond Formation/ Cleavage in [Re(bpy)(CO)3]2 Different from That in [Re(CO)5]2? Experimental and Theoretical Studies on the Dimers and Fragments. *Inorg. Chem.* **2004**, 43 (24), 7636–7647.
- (44) Hayashi, Y.; Kita, S.; Brunschwig, B. S.; Fujita, E. Involvement of a Binuclear Species with the Re–C(O)O–Re Moiety in CO2 Reduction Catalyzed by Tricarbonyl Rhenium(I) Complexes with Diimine Ligands: Strikingly Slow Formation of the Re–Re and Re–

- C(O)O-Re Species from Re(dmb)(CO)3S (dmb = 4,4'-Dimethyl-2,2'-bipyridine, S = Solvent). *J. Am. Chem. Soc.* **2003**, 125 (39), 11976–11987.
- (45) Stanton, C. J., 3rd; Machan, C. W.; Vandezande, J. E.; Jin, T.; Majetich, G. F.; Schaefer, H. F., 3rd; Kubiak, C. P.; Li, G.; Agarwal, J. Re(I) NHC Complexes for Electrocatalytic Conversion of CO2. *Inorg. Chem.* **2016**, *55* (6), 3136–3144.
- (46) Riplinger, C.; Carter, E. A. Influence of Weak Brønsted Acids on Electrocatalytic CO2 Reduction by Manganese and Rhenium Bipyridine Catalysts. *ACS Catal.* **2015**, *5* (2), 900–908.
- (47) Doud, E. A.; Inkpen, M. S.; Lovat, G.; Montes, E.; Paley, D. W.; Steigerwald, M. L.; Vázquez, H.; Venkataraman, L.; Roy, X. In Situ Formation of N-Heterocyclic Carbene-Bound Single-Molecule Junctions. J. Am. Chem. Soc. 2018, 140 (28), 8944–8949.
- (48) Palasz, J. M.; Long, Z.; Meng, J.; Videla, P. E.; Kelly, H. R.; Lian, T.; Batista, V. S.; Kubiak, C. P. A Resilient Platform for the Discrete Functionalization of Gold Surfaces Based on N-Heterocyclic Carbene Self-Assembled Monolayers. *J. Am. Chem. Soc.* **2024**, *146* (15), 10489–10497.
- (49) MacLeod, M. J.; Goodman, A. J.; Ye, H.-Z.; Nguyen, H. V. T.; Van Voorhis, T.; Johnson, J. A. Robust gold nanorods stabilized by bidentate N-heterocyclic-carbene—thiolate ligands. *Nat. Chem.* **2019**, *11* (1), 57–63.
- (50) DeJesus, J. F.; Sherman, L. M.; Yohannan, D. J.; Becca, J. C.; Strausser, S. L.; Karger, L. F. P.; Jensen, L.; Jenkins, D. M.; Camden, J. P. A Benchtop Method for Appending Protic Functional Groups to N-Heterocyclic Carbene Protected Gold Nanoparticles. *Angew. Chem., Int. Ed.* **2020**, *59* (19), 7585–7590.
- (51) Gorodetsky, B.; Ramnial, T.; Branda, N. R.; Clyburne, J. A. C. Electrochemical reduction of an imidazolium cation: a convenient preparation of imidazole-2-ylidenes and their observation in an ionic liquid. *Chem. Commun.* **2004**, No. 17, 1972–1973.
- (52) Aydogan Gokturk, P.; Donmez, S. E.; Ulgut, B.; Türkmen, Y. E.; Suzer, S. Optical and XPS evidence for the electrochemical generation of an N-heterocyclic carbene and its CS2 adduct from the ionic liquid [bmim][PF6]. *New J. Chem.* **2017**, *41* (18), 10299–10304
- (53) Pinson, J.; Podvorica, F. Attachment of organic layers to conductive or semiconductive surfaces by reduction of diazonium salts. *Chem. Soc. Rev.* **2005**, *34* (5), 429–439.
- (54) Bélanger, D.; Pinson, J. Electrografting: a powerful method for surface modification. *Chem. Soc. Rev.* **2011**, *40* (7), 3995–4048.
- (55) Amit, E.; Dery, L.; Dery, S.; Kim, S.; Roy, A.; Hu, Q.; Gutkin, V.; Eisenberg, H.; Stein, T.; Mandler, D.; et al. Electrochemical deposition of N-heterocyclic carbene monolayers on metal surfaces. *Nat. Commun.* **2020**, *11* (1), 5714.
- (56) Yamada, T.; Tominari, Y.; Tanaka, S.; Mizuno, M. Infrared Spectroscopy of Ionic Liquids Consisting of Imidazolium Cations with Different Alkyl Chain Lengths and Various Halogen or Molecular Anions with and without a Small Amount of Water. J. Phys. Chem. B 2017, 121 (14), 3121–3129.
- (57) Bard, A. J.; Faulkner, L. R. Electrochemical Methods: Fundamentals and Applications; Wiley, 2000.
- (58) Stoneham, A. M. Shapes of Inhomogeneously Broadened Resonance Lines in Solids. *Rev. Mod. Phys.* **1969**, 41 (1), 82–108.
- (59) Clark, M. L.; Rudshteyn, B.; Ge, A.; Chabolla, S. A.; Machan, C. W.; Psciuk, B. T.; Song, J.; Canzi, G.; Lian, T.; Batista, V. S.; et al. Orientation of Cyano-Substituted Bipyridine Re(I) fac-Tricarbonyl Electrocatalysts Bound to Conducting Au Surfaces. *J. Phys. Chem. C* 2016, 120 (3), 1657–1665.
- (60) Zamlynny, V.; Lipkowski, J. Quantitative SNIFTIRS and PM IRRAS of Organic Molecules at Electrode Surfaces. In *Advances in Electrochemical Science and Engineering*: John Wiley and Sons, 2006; pp 315–376
- (61) Elgrishi, N.; Rountree, K. J.; McCarthy, B. D.; Rountree, E. S.; Eisenhart, T. T.; Dempsey, J. L. A Practical Beginner's Guide to Cyclic Voltammetry. *J. Chem. Educ.* **2018**, 95 (2), 197–206.

- (62) Huffman, B. L.; Bredar, A. R. C.; Dempsey, J. L. Origins of non-ideal behaviour in voltammetric analysis of redox-active monolayers. *Nat. Rev. Chem.* **2024**, *8* (8), 628–643.
- (63) Yu, Z. L.; Casanova-Moreno, J.; Guryanov, I.; Maran, F.; Bizzotto, D. Influence of Surface Structure on Single or Mixed Component Self-Assembled Monolayers via in Situ Spectroelectrochemical Fluorescence Imaging of the Complete Stereographic Triangle on a Single Crystal Au Bead Electrode. *J. Am. Chem. Soc.* **2015**, *137* (1), 276–288.
- (64) Doneux, T.; Steichen, M.; De Rache, A.; Buess-Herman, C. Influence of the crystallographic orientation on the reductive desorption of self-assembled monolayers on gold electrodes. *J. Electroanal. Chem.* **2010**, 649 (1), 164–170.
- (65) Guerra, E.; Kelsall, G. H.; Bestetti, M.; Dreisinger, D.; Wong, K.; Mitchell, K. A. R.; Bizzotto, D. Use of Underpotential Deposition for Evaluation of Overpotential Deposition Kinetics of Reactive Metals. *J. Electrochem. Soc.* **2004**, *151* (1), No. E1.
- (66) Huffman, B. L.; Donley, C. L.; Dempsey, J. L. Electrochemistry of Redox Active Ferrocene Covalently Attached to Glassy Carbon Electrodes. *J. Electrochem. Soc.* **2023**, *170* (12), 126501.
- (67) Rountree, E. S.; McCarthy, B. D.; Eisenhart, T. T.; Dempsey, J. L. Evaluation of Homogeneous Electrocatalysts by Cyclic Voltammetry. *Inorg. Chem.* **2014**, 53 (19), 9983–10002.
- (68) Savéant, J.-M.; Costentin, C. Elements of Molecular and Biomolecular Electrochemistry; John Wiley and Sons, 2019.
- (69) Costentin, C.; Drouet, S.; Robert, M.; Saveant, J. M. Turnover numbers, turnover frequencies, and overpotential in molecular catalysis of electrochemical reactions. Cyclic voltammetry and preparative-scale electrolysis. *J. Am. Chem. Soc.* **2012**, *134* (27), 11235–11242.
- (70) Inayeh, A.; Groome, R. R. K.; Singh, I.; Veinot, A. J.; de Lima, F. C.; Miwa, R. H.; Crudden, C. M.; McLean, A. B. Self-assembly of N-heterocyclic carbenes on Au(111). *Nat. Commun.* **2021**, *12* (1), 4034
- (71) Bhattacharyya, D.; Videla, P. E.; Palasz, J. M.; Tangen, I.; Meng, J.; Kubiak, C. P.; Batista, V. S.; Lian, T. Sub-Nanometer Mapping of the Interfacial Electric Field Profile Using a Vibrational Stark Shift Ruler. *J. Am. Chem. Soc.* **2022**, *144* (31), 14330–14338.
- (72) Goldsmith, Z. K.; Secor, M.; Hammes-Schiffer, S. Inhomogeneity of Interfacial Electric Fields at Vibrational Probes on Electrode Surfaces. *ACS Cent. Sci.* **2020**, *6* (2), 304–311.
- (73) Pavlishchuk, V. V.; Addison, A. W. Conversion constants for redox potentials measured versus different reference electrodes in acetonitrile solutions at 25°C. *Inorg. Chim. Acta* **2000**, 298, 97–102.
- (74) Dominique, N. L.; Chandran, A.; Jensen, I. M.; Jenkins, D. M.; Camden, J. P. Unmasking the Electrochemical Stability of N-Heterocyclic Carbene Monolayers on Gold. *Chem. Eur. J.* **2024**, *30* (15), No. e202303681.